JOURNAL OF GEOPHYSICAL RESEARCH, VOL. 105, NO. C3, PAGES 6541–6548, MARCH 15, 2000

Ice growth and solar heating in springtime leads

D. K. Perovich and J. A. Richter-Menge

U. S. Army Cold Regions Research and Engineering Laboratory, Hanover, New Hampshire

Abstract. The large thermal contrast between the cold atmosphere and the relatively warm ocean in springtime leads results in rapid ice growth and large fluxes of heat from the ocean to the atmosphere and of salt from the ice to the ocean. However, the magnitude of the ice growth and of the fluxes is moderated by solar radiation absorbed in the ice and upper ocean. During the Arctic lead experiment (LeadEx) we monitored ice conditions at four springtime leads during the first few days of growth. The experiment took place in March–April 1992 in the Beaufort Sea (73°N, 146°W). Two of the leads were <200 m in width, one was approximately a kilometer wide, and the fourth was quite large, more than a few kilometers wide. Ice thickness typically increased rapidly, with 15–20 cm of growth in the first few days. The crystallographic analysis of a series of ice cores taken across and along the edge of one of the smaller leads indicated that granular ice was more abundant along the edges (30%) of the lead than in the central part of the lead (10%). Observations suggest that thermodynamics processes dominated ice growth in these leads. Additional thickening of the ice at the edge of the leads was common because of rafting of the young ice and the accumulation of blowing snow. Ice temperature profiles exhibited a diurnal cycle induced by solar radiation, with daily oscillations of roughly 5°C observed in the interior of the lead ice. Theoretical simulations for one lead indicated that during the first few days of ice growth, 30% of the incident solar irradiance was absorbed in the ice and 25% was absorbed in the upper ocean. The total amount of solar energy absorbed in the ice during this period was roughly equivalent to 4 cm of ice growth. The solar heating in ice and water is roughly comparable in magnitude to the net longwave and is approximately two thirds of the turbulent fluxes.

1. Introduction

During the ice growth season, open leads provide a large thermal contrast between the cold atmosphere and the relatively warm ocean. This contrast results in large fluxes of heat from the ocean to the atmosphere and, consequently, rapid ice growth. Earlier studies have indicated that even though leads and young ice typically constitute only a small fraction of the ice cover, they significantly impact the thermodynamics of the ice cover [*Badgley*, 1966; *Maykut*, 1978, 1982; *Gow et al*., 1990] as well as the thermohaline structure of the upper ocean [*Smith et al*., 1990; *Morison et al*., 1992]. Leads cause perturbations in both the atmosphere and ocean. The heat released into the atmosphere can result in forced convection [*Schnell et al*., 1989; *Pinto et al*., 1995; *Pinto and Curry*, 1995], while the dense brine rejected by the growing ice causes mixing in the upper ocean [*Smith*, 1973; *Smith et al*., 1990; *Morison et al*., 1992].

Because of this importance, the Office of Naval Research sponsored a 5-year interdisciplinary study of springtime leads called LeadEx [*The LeadEx Group*, 1993]. The goal of this work was to develop an understanding of the processes of springtime leads and their impact on the atmosphere and ocean. Two field experiments in the springs of 1991 and 1992 were central components of this study. Research on the upper ocean, the lower atmosphere, and the ice cover was conducted during LeadEx. Our effort was primarily concerned with ice growth in leads, the physical properties of lead ice, and salt fluxes from the growing ice to the upper ocean.

Paper number 1999JC900321.

Ice growth in leads and polynas has been investigated in field and modeling studies. *Martin and Kauffman* [1981] describe the commonly observed development of grease ice in leads and polynyas under windy conditions. Their model indicates that grease ice forms when frazil particles are herded together as a result of wind waves and wind-driven surface currents. *Bauer and Martin* [1983] suggest that in leads <500 m, ice growth under these conditions is an order of magnitude greater than one-dimensional ice growth and can significantly increase the heat and salt flux. Rapid desalination of sea ice within the first week of growth has been associated with rapid ice growth formation on the basis of results from investigations like that of *Nakawo and Sinha* [1981], who observed a time series of vertical temperature profiles in first-year sea ice.

On the basis, in part, of these earlier studies our expectations prior to the field experiment were straightforward. We believed that springtime leads were areas with great amounts of frazil ice production and tremendous heat fluxes from the ocean to the atmosphere. However, the observations we made during LeadEx indicate that this simple picture is incomplete and that the actual behavior of springtime leads is more complex. In this paper we use field observations from four springtime leads, along with a radiative transfer model, to explore ice production in leads and the impact of solar radiation on springtime leads.

2. Field Experiment

LeadEx was a large interdisciplinary program directed at assessing the impact of leads on the atmosphere and ocean and understanding the processes of heat transfer to the atmosphere and salt to the upper ocean associated with freezing leads. The research team included oceanographers, atmospheric scientists, microwave remote sensing researchers, and ice physicists. Be-

Table 1. Summary of the Meteorological Conditions Present During the Lead Investigations and the Ice Characteristics of Each Lead

	Time	Width	T_a, °C	u, m s^{-1}	F_r, W m^{-2}	H_f, cm	S_f, o/oo	%C	%G
Pilot lead	April 14–21	200 m	−12.5–−26.5	Light	?	17	7.3	72	28
Lead 3	April 6–9	1 km	−21–−26	2.5–6.5	120–160	19	13.6	82	18
Lead 4	April 11–13	200 m	−20–−30	4–5	145	16	25.1	71	29
Lead 5 (up/down)	April 17	many km	−21	10	185	21 / 16	17.2 / 15.3	0 / 0	100 / 100

These data include the range of daily averages for air temperature T_a, wind speed at 2 m above the ice surface (u), and the incoming solar radiation F_r compiled from measurements presented by *Ruffieux et al*. [1995]. The final ice thickness H_f and bulk salinity S_f are presented as are the relative percentages of columnar (%C) and granular (%G) ice in cores taken from the lead ice.

cause of the paucity of observational data, LeadEx focused on two field efforts: a pilot study in April 1991 and a main experiment in late March and April 1992. This field work took place in the Beaufort Sea, ~250 km north of Prudhoe Bay, Alaska (72°N, 144°W). An overview of the experimental approach and results is presented by *The LeadEx Group* [1993].

We studied four leads that encompassed the range of Arctic lead conditions present in late winter and early spring. In the pilot experiment we monitored for 1 week a 200-m-wide lead that underwent a modest amount of deformation. Measurements were made at three leads during the main experiment. We spent 3 days studying a 1 km wide lead with little deformation, 2 days watching a 100-m-wide lead where there was considerable deformation, and a brief few hours visiting a several kilometer–wide lead where ice was forming in the presence of moderate winds. The meteorological conditions and basic ice properties of these four leads are summarized in Table 1.

The focus of our work was on the ice, specifically its growth and properties. Ice thicknesses and growth rates were measured by periodically drilling holes in the lead ice. In addition, 10-cm-diameter cores were removed from the ice and analyzed to determine the salinity, brine volume, and crystallographic structure of the lead ice [*Perovich and Richter-Menge*, 1994]. These cores were typically taken 1–2 m from the edge of the newly forming ice since the new ice was often too thin to stand on. Ice salinities were determined by cutting the cores into sections that were 0.02–0.10-m-long and then melting the sections in a closed container. The salinity of the meltwater was measured to a precision of ±0.2 parts per thousand (ppt) using a Beckman Solubridge. Ice cores were shipped back to Cold Regions Research and Engineering Laboratory (CRREL) for crystallographic analysis in an insulated box cooled with dry ice. The crystallographic structure of the lead ice was determined by examining horizontal and vertical thin sections of this ice under crossed Polaroids [*Tucker et al*., 1987]. Ice surface conditions, including the formation and evolution of frost flowers, were closely monitored by measuring surface temperature and salinity, sampling frost flowers, and taking photographs [*Perovich and Richter-Menge*, 1994].

Temperatures in the lead ice were measured at pilot lead, lead 3, and lead 4 using thermistor strings. These strings were frozen into the growing lead ice and extended from 5 to 10 cm above the ice surface, through the ice, and 20 to 30 cm into the upper ocean. The thermistor spacing was 1 cm within the ice and every 5 cm in the air and ocean. Temperatures were automatically recorded on a Campbell CR-10 data logger every 30 min. The precision of the thermistors was ±0.1°C.

3. Results and Discussion

3.1. Ice Production

Vertically oriented, columnar crystals accounted for 70–80% of the ice structure in the cores taken from pilot lead, lead 3, and lead 4 (Table 1). Figure 1 presents a core from lead 3, illustrating the ice structure typically observed in all of these leads. This 19-cm-thick core was taken at the edge of the newly forming ice cover 4 days after the lead had developed. At the top of the core there is a 1-cm-thick layer of granular ice, which transitions to a 3-cm-thick layer of columnar ice. Alternating thin bands of granular and columnar ice crystals continue to a depth of 8 cm, ranging in thickness from 0.5 to 3 cm. The bottom 11 cm of the core has a columnar structure. The horizontal thin section taken at a 14-cm depth shows that the columnar crystals had already become aligned in the horizontal plane of this newly forming ice cover.

The predominance of columnar crystals suggests that the majority of ice in these leads was formed under conditions where the latent heat flow was one-dimensional through the thickness of the ice cover [*Weeks and Ackley*, 1986]. This type of growth occurs after an initial ice cover has formed. The initial layer of ice typically consists of randomly oriented granular crystals. The thickness of the top granular layer provides some insight into the level of turbulence in the upper layer of the ocean during the initial growth phase. A thin layer of granular ice, like the ones we observed at these leads, implies that the new ice grew under relatively quiet conditions. The light wind conditions reported during the measurement periods at each of these leads are consistent with this observation (Table 1).

There are two possible explanations for the bands of granular ice often seen in the lead ice cores. Granular ice at depth has been associated with the advection of frazil ice crystals under the newly formed ice. *Gow et al*. [1990] present an example of ice produced under these conditions. They reported a layer of granular ice that extended from 8 to 50 cm in a core taken from young ice growing in a lead. This ice growth occurred after the lead reopened, during a period of significant winds. Model studies by *Bauer and Martin* [1983] suggest that significant amounts of frazil ice can be generated in small leads when strong, cold winds blow over the open water. The frazil ice produced under these conditions is then blown downwind and collects against the side of the thick ice adjacent to the lead, forming a wedge of granular ice. As we have mentioned, the necessary condition of high winds was not present at the pilot lead, lead 3, or lead 4.

Rafting of the young ice is another mechanism that can result in alternating layers of granular and columnar ice. In the leads we observed this was a common occurrence, particularly near the edges of the leads. As the thicker floes of ice on either side of the lead move relative to one another, the thinner, weaker ice in the lead deforms. Under conditions of compression or shear this can result in large sections of the thin ice riding up on one another.

Pilot lead provided our longest observation period, which was 7 days. In this time the ice grew thick enough to walk across, allowing us to conduct two core transects to investigate ice structure variability. Cores were taken along lines running

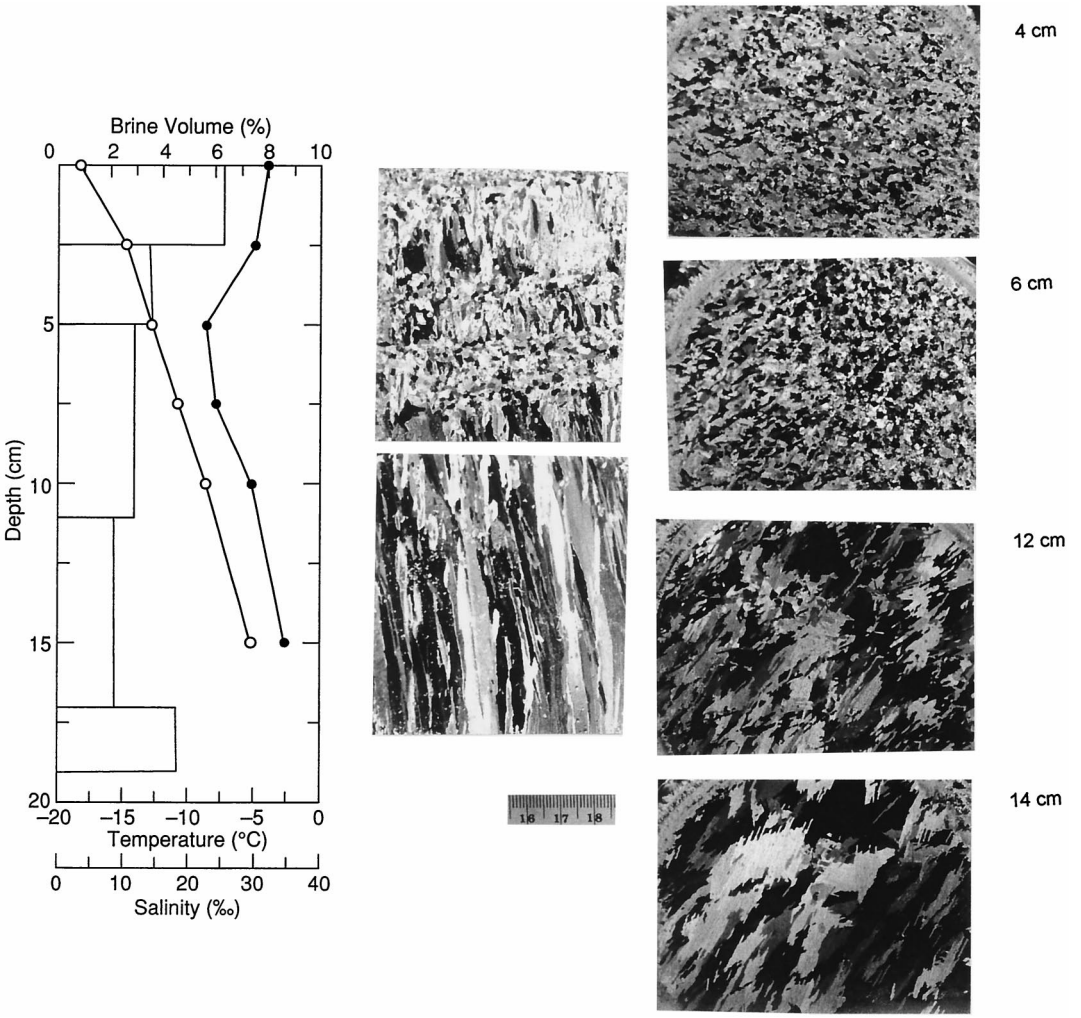

Figure 1. Vertical profiles of ice temperature (open circles), salinity (bars), and brine volume (solid circles) for lead 3. Thin section photographs showing the vertical profile of the ice crystal structure as well as horizontal cross sections are also presented (scale in centimeters).

parallel (3.5 m from the lead edge) and perpendicular to the edge of the lead. The ice at both edges of the young ice was visibly deformed. Plates of thin ice, stacked up on one another, were apparent on the right-hand side of the lead, where one of the transect lines was located. On the other side of the lead, blocks of thick and thin ice were incorporated into the new ice cover. The ice at the center of the lead had a smooth, flat surface, indicating that it was undeformed.

The thickness and structural characteristics of the ice cores collected from this lead are consistent with these initial visual observations. At the center of the lead the ice thickness and structure was extremely uniform. Four days after the lead had formed, the ice was ~15 cm thick. The top 1–3 cm of the ice had a granular texture, and the remainder of the core was columnar. At the edges, where deformation was evident, there was significant spatial variability in both ice thickness and structure. The ice thickness ranged from ~15 to 45 cm. Rafting was evident from the relatively thin layers of granular ice between thicker layers of columnar ice. The thickness of the granular layers in the cores from the deformed sections of the lead was comparable to the thickness of the granular layer at the top of the ice cores taken in the undeformed center portion of the lead. The transitions between granular and columnar ice structure typically were abrupt and horizontally oriented. Both of these observations suggest stacking of pieces of the new ice.

Deformation of the ice near the edges of the lead creates localized areas where the ice thickness is significantly greater than in undeformed regions. In the case of pilot lead, there were locations where the deformed ice was more than twice the thickness of the undeformed ice. The resulting increase in ice thickness at the edges of the lead can be comparable to the effect that wind-herded frazil is expected to have on ice thickness variations. The *Bauer and Martin* [1983] model of grease ice growth indicates that in a 200-m-wide lead, with winds speeds of 10 m s^{-1} and an air temperature of −20°C, the average ice thickness of the frazil ice would be twice that of ice grown under quiet conditions.

Another potential source of ice production along the edge of the lead is drifting snow. Snowdrifts commonly develop at the lead edge, even under light wind conditions. If the weight of the snow on the thin ice becomes adequate, it can depress the surface of the thin ice below its freeboard. This causes flooding of the snow, which quickly freezes. The resulting snow ice has a granular structure. The thickness of the snow ice layer ice is variable since the wind-driven distribution of snow is nonuniform. Given the snowdrifts that developed on the upwind side of pilot lead, it is likely that much of the 1–10 cm of granular

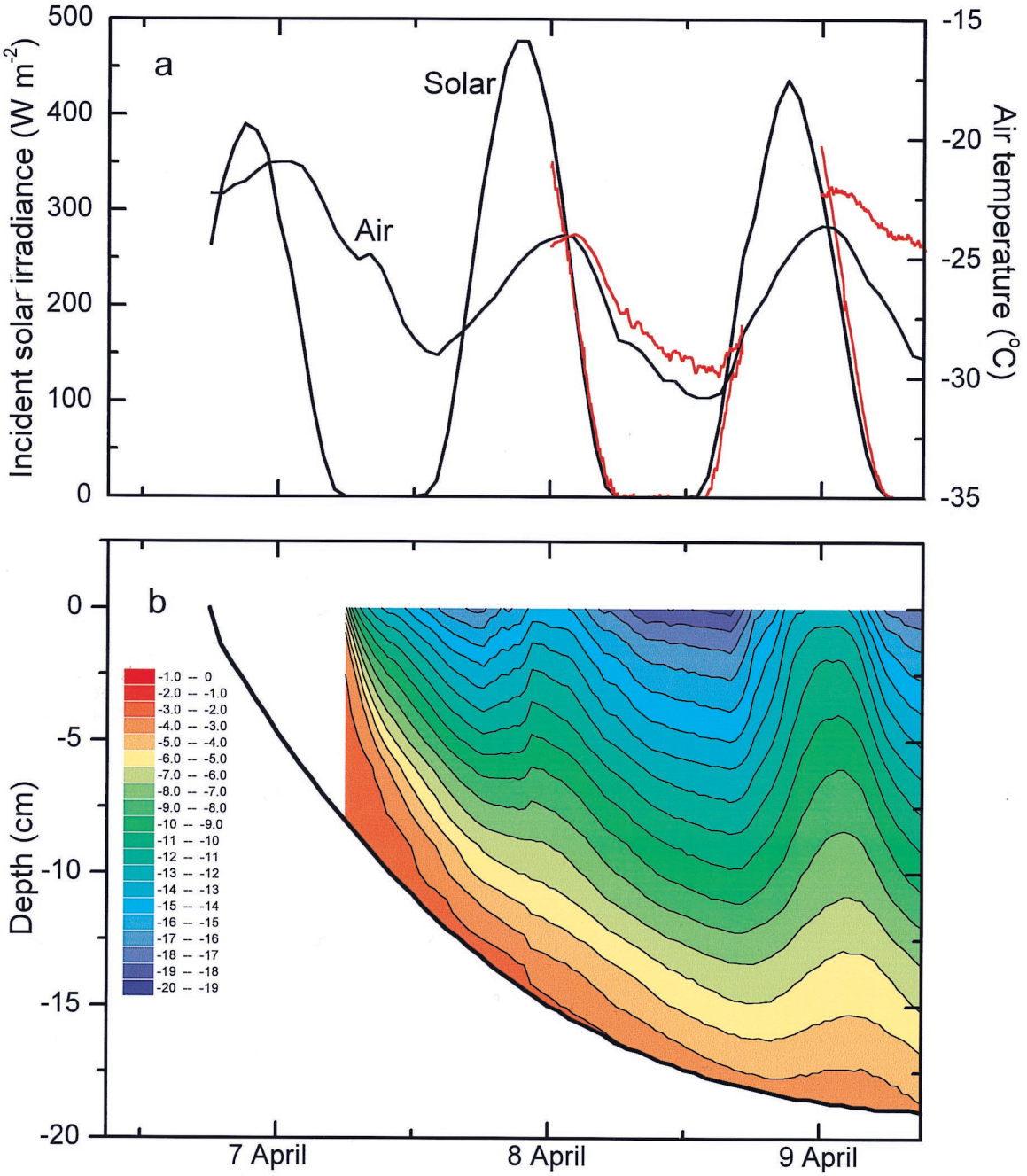

Plate 1. Time series results from lead 3: (a) observations of incident solar irradiance and air temperature (C. Fairall, personal communication, 1997) and (b) measurements of ice growth and internal temperature. In Plate 1a the incident solar irradiance and the air temperature were both measured at the main camp. The red lines denote incident irradiance and air temperature measured at lead 3. Time is UT, not local time.

ice found in cores there was snow ice. *Gow et al*. [1990] suggest that snow ice was the primary reason for spatial variability in the granular content of ice cores taken in their primary lead, which developed during light wind conditions.

The structural characteristics of the ice cores taken from pilot lead, lead 3, and lead 4 suggest that frazil ice production was not significant in these leads, where ice growth occurred under light winds conditions. We observed considerable frazil ice growth once during LeadEx. This was at lead 5, which was several kilometers wide and developed when sustained winds speeds were relatively high, at ~10 m s^{-1}, and had been high for several days. The air temperature was −21°C. Wind herding of frazil against the thicker ice on the downwind side of the lead was clearly evident. Ice cores taken at the downwind and upwind edges of the lead only consisted of frazil ice. Significant frazil production in a lead that develops under these conditions is anticipated on the basis of the work of *Martin and Kauffman* [1981]. However, during the LeadEx pilot and main field experiments the conditions necessary to produce large quantities of frazil were rarely present.

3.2. Ice Growth, Temperature, and Solar Heating

Time series measurements of ice temperature and growth were made at pilot lead, lead 3, and lead 4. To illustrate the major features of ice growth, temperature, and solar heating in

these three leads, we will examine results from lead 3. The time series of incident solar irradiance F_r and air temperature T_a measured during the lead 3 deployment are plotted in Plate 1a (C. Fairall, personal communication, 1997). These data are a mix of observations made at lead 3 and at the base camp. Since the time series of meteorological data measured at lead 3 was incomplete, observations made at the base camp were used to fill the gaps. As Plate 1a illustrates, comparisons between simultaneous observations showed that incident solar irradiances at lead 3 and base camp are within a few percent. The air was somewhat colder (1°–3°C) over the multiyear ice at the main camp compared to the thin ice at the lead, consistent with the observations of *Ruffieux et al*. [1995]. Air temperatures at lead 3 were low, ranging from a maximum of −21°C to a minimum of −31°C and averaging −26°C. There was a diurnal variation of ~5°C. Skies were clear, and the incident solar irradiance was considerable. There was a strong diurnal signal in F_r, with peak values of 400–500 W m^{-2} at solar noon and a few hours of darkness each night (F_r = 0 W m^{-2}). The average value of F_r during the lead 3 measurements was 170 W m^{-2}.

Contours of ice internal temperatures at lead 3, measured using the thermistor string, are plotted in Plate 1b. These temperatures were measured in the lead ice a few meters from the edge of the multiyear floe. The heavy solid line denotes the position of the bottom of the ice. During the 2.5 days of the deployment the ice grew to a thickness of 19 cm. Ice growth was initially rapid, with growth rates of ~1 cm h^{-1} in the first hours followed by a gradual decrease to 0.1 cm h^{-1} by the end of the second day. As expected, there is a general cooling trend in the ice as it grows thicker. Superposed over this cooling trend was a strong diurnal signature, with significant daytime warming of the ice associated with the cycle of F_r and T_a. Even with this warming, the ice was still cold enough that there was accretion on the bottom. However, growth rates did decrease during the day, as the conductive flux near the ice bottom decreased from 150 to 80 W m^{-2} as the ice warmed. The conductive fluxes in the ice were computed from the temperature profiles using $F = -k(\Delta T_i/\Delta z)$, where $\Delta T_i/\Delta z$ is the vertical (z) ice temperature (T_i) gradient. The thermal conductivity of sea ice k is computed using

$$k = k_i + \frac{\beta S}{T_i - 273},$$

where k_i is the thermal conductivity of fresh ice (2.03 W m^{-1} K^{-1}), T_i is the ice temperature (kelvins), S is the salinity (ppt), and β is a constant (0.117 W m^{-1} ppt^{-1}) [*Untersteiner*, 1961].

This diurnal warming is illustrated by the two temperature profiles plotted in Figure 2. These were the coldest (0800 LT) and warmest (1700 LT) profiles of April 8, 1992. The warming was as large as 7°C near the surface and 4°C at a depth of 10 cm. This represents a significant amount of heat input to the ice. The change in heat content Q_s associated with this warming is

$$Q_s = \rho \int \int c_s dT_i dz, \qquad (1)$$

where ρ is the sea ice density (900 kg m^{-3}) and c_s is the ice specific heat. We use *Schwerdtfeger*'s [1963] expression for the specific heat of sea ice:

$$c_s = \frac{-S_i L}{\alpha T_i^2} + \frac{S_i(c_w - c_i)}{\alpha T_i} + c_i,$$

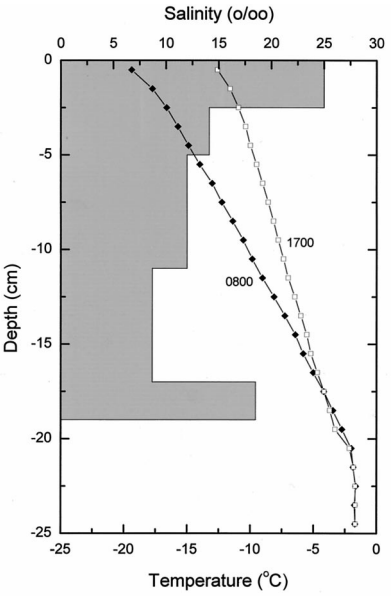

Figure 2. Solar warming of the young ice at lead 3. Plotted are the vertical profiles of the daily minimum and maximum ice temperature measured at 0800 and 1700 LT on April 8, 1992, respectively. The salinity profile of the ice is denoted by the shaded area.

where α is a constant (−0.0182°C^{-1}), L is the latent heat of fusion of pure ice (333.9 kJ kg^{-1}), c_w is the specific heat of water (4.23 kJ°C^{-1} kg^{-1}), c_i is the specific heat of ice (2.01 kJ°C^{-1} kg^{-1}), and S_i is the ice salinity. Using the two temperature profiles and the ice salinity profile from Figure 2 as input to (1), we computed Q_s for the top 15 cm of the lead ice. The increase in heat content was 2 MJ m^{-2}, which was equivalent to a heat flux of 63 W m^{-2}.

Is solar energy absorbed in the lead ice the source of this heat? Unfortunately, we do not have any observations of the partitioning of the incident solar irradiance between reflection, absorption in ice, and transmission to the ocean to address this question directly. However, we can use a radiative transfer model to assess the impact of solar radiation on the young ice and the upper ocean. A two-stream, multilayer, spectral, visible, and near-infrared radiative transfer model [*Dunkle and Bevans*, 1957; *Grenfell*, 1979; *Perovich*, 1990] was used in conjunction with observations of ice physical properties and the incident solar irradiance F_r to calculate the amount of solar irradiance reflected (αF_r), absorbed in the ice ($A_i F_r$), and deposited in the water column ($F_r(1 - \alpha - A_i)$). The optical properties of the ice cover were represented using extinction coefficients for young ice [*Perovich and Grenfell*, 1981]. Frost flower growth on the newly forming ice was ubiquitous during this study [*Perovich and Richter-Menge*, 1994]. Laboratory optical studies showed that the presence of frost flowers on young ice caused an increase of 0.1–0.2 in albedo [*Grenfell et al*., 1998]. Their influence was simulated by adding a thin surface layer with the optical properties of wet snow [*Grenfell and Maykut*, 1977]. Extinction coefficients for very clear water were used to represent the optical properties of the upper ocean [*Tyler and Smith*, 1970; *Grenfell*, 1979; *Smith and Baker*, 1981]. These optical properties were combined with observations of ice thickness, incident solar irradiance [*Ruffieux et al*., 1995; C. Fairall, personal communication, 1997], and sky conditions to provide the model input parameters. The model computes both spectral and wavelength-integrated values of albedo and transmittance.

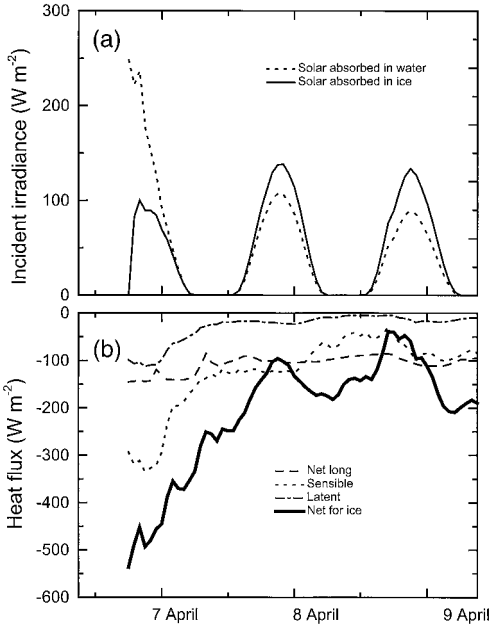

Figure 3. Time series results from lead 3: (a) calculated values of the solar irradiance absorbed in the ice and in the water and (b) estimates of the net longwave fluxes, turbulent fluxes, and overall energy balances. Time in UT, not local time.

Figure 3a shows the results of these calculations in the form of a time series of solar radiation absorbed in the water and in the ice. Initially, with the low albedo of open water and the timing being near solar noon the flux of solar radiation into the upper ocean was large, over 200 W m^{-2}. The albedo increased quickly from an open water value of 0.05 to 0.5 by daybreak on April 7. This increase was a result of the rapid initial ice growth plus an enhancement of albedo due to the formation of frost flowers on the ice surface. The ice thickness increased to more than 10 cm during April 7, which was the second day of ice growth. As a result of the increase in albedo and the increase in ice thickness, there was an increase in the incident solar radiation reflected to ~50%, an increase in the amount absorbed in the ice to ~30%, and consequently, a decrease in the solar radiation deposited in the upper ocean to ~20%. From this point more of the incident solar radiation was absorbed in the ice than in the water. Maximum values of the shortwave flux absorbed in the ice were near 120 W m^{-2}. For the period between 0800 and 1700 hours on April 8 (Figure 2) the average solar flux absorbed in the ice was 105 W m^{-2}. This was in excess of the 63 W m^{-2} needed for the warming of the ice, implying that solar heating contributed significantly to the warming of the ice.

The theoretical estimate of the amount of shortwave radiation absorbed in the upper ocean after the ice cover had begun to develop compares well with direct measurements of the ocean heat made by *McPhee and Stanton* [1996]. They report results from two techniques to measure the downward turbulent heat flux: a vertical array of four turbulence-measuring instrument clusters and an automated, loose-tethered microstructure profiler. Results from both instruments indicate that at midday, 10–20% of the incident shortwave radiation passed through the ice cover into the water column. Maximum values of the heat flux in the water were ~50 W m^{-2} and extended down to over 20 m as a result of turbulent mixing.

For at least part of the day the flux of shortwave radiation absorbed in the lead ice is considerable. To provide a context for, and to assess the relative importance of, the solar heat flux, we need to examine the other components of the ice energy balance: the turbulent and longwave fluxes. Determining the sensible and latent heat fluxes over young lead ice is quite difficult because of the spatial and temporal variability in air temperature, surface temperature, wind speed, and humidity. A detailed study of the energy fluxes was made for lead 4 but not for lead 3 [*Ruffieux et al*., 1995]. Our intent in this study is more limited in that we merely wish to generate a rough estimate of the sensible and latent heat fluxes for comparison to the solar radiation flux. Consequently, we made several simplifications. No attempt was made to estimate the spatial variability of the fluxes across the lead. Such an effort is well beyond the scope of this study. Since the ice thickness and properties at the thermistor site were representative of the lead as a whole, the surface temperature T_s measured at the thermistor string was used for the entire lead. The time series of incoming solar irradiance, incoming longwave irradiance $F_{L\downarrow}$, 2-m air temperature T_a, wind speed u, and relative humidity (r—a fraction between 0 and 1) are a combination of values measured at lead 3 and at the main camp. The greatest uncertainty from this simplification will probably be overestimating of the turbulent fluxes. Some error was introduced when air temperatures over the thick ice at the main camp were substituted for missing lead values. Camp air temperatures typically were 1°–3°C colder than those over the thin lead ice [*Ruffieux et al*., 1995], corresponding to an overestimate of sensible heat flux of 10–20 Wm^{-2}.

The sensible heat is calculated using

$$F_s = \rho_a c_s c_p u (T_a - T_s),$$

where c_s is the bulk transfer coefficient for sensible heat and c_p is the specific heat of air at constant pressure (1004 J kg^{-1}°C^{-1}). A fourth-order polynomial approximation is used for the latent heat flux [*Maykut*, 1978]:

$$F_e = \frac{0.622 \rho_a L_v c_e u}{p} [a_1(rT_a^4 - T_s^4) + a_2(rT_a^3 - T_s^3) + a_3(rT_a^2 - T_s^2) + a_4(rT_a - T_s) + a_5(r - 1)],$$

where ρ_a is the density of air (0.0013 g cm^{-2}), L_v is the latent heat of fusion (596 cal g^{-1}), and p is the surface pressure in millibars. *Andreas and Murphy* [1986] developed a methodology to determine the bulk transfer coefficients for sensible heat c_s and latent heat c_e in the internal boundary layer over leads. The height of the internal boundary layer (Z_i) over a lead is related to the fetch X across the lead by $Z_i = 0.82 \ln X + 0.02$ [*Andreas and Cash*, 1999]. Z_i is greater than the height of our meteorological measurements (2 m) for leads wider than 11 m [*Andreas and Cash*, 1999]. Since lead 3 was much wider than this, we apply the *Andreas and Murphy* [1986] formulation and determine that $c_s = c_e = 0.00214$. The constants in the polynomial are $a_1 = 2.78798202 \times 10^{-6}$, $a_2 = -0.0026913395$, $a_3 = 0.97920849$, $a_4 = -158.63779$, and $a_5 = 9653.1925$.

The net longwave radiation F_L is simply the difference between the incoming ($F_{L\downarrow}$) and the outgoing ($F_{L\uparrow}$) longwave radiation. The incoming longwave radiation was obtained from observations made at lead 3 and at the main camp [*Ruffieux et al*., 1995; C. Fairall, personal communication, 1997]. The outgoing longwave radiation was computed using the Stefan Boltzmann equation $F_{L\downarrow} = \varepsilon \sigma T_s^4$, where the emissivity $\varepsilon = 1$

[*Grenfell et al.*, 1998], the Stefan-Boltzmann constant $\sigma = 5.67 \times 10^{-8}$ W m^{-2} K^{-4}, and T_s is the surface temperature measured at the thermistor string.

The net heat flux into the ice, determined by summing the net shortwave radiation, the net longwave radiation, and the turbulent fluxes, is plotted in Figure 3b.

$$F_{\text{net}} = A_i F_r + F_s + F_e + F_{L\downarrow} - F_{L\uparrow}$$

The behavior of the net heat flux over time is as expected (Figure 3b): large initial losses to the atmosphere slowly decrease with time as the ice grows thicker and the thermal contrast between the ice surface and atmosphere is reduced. Again, it should be noted that the net flux as calculated here is probably an overestimate since the presence of the lead would moderate air temperatures compared to those over the multiyear ice at the base camp, reducing the turbulent fluxes. The effect of solar heating on the net heat flux for the ice is evident in Figure 3b. While the net flux is always negative and rather large for the entire 2.5-day observation period, there is a significant diurnal oscillation of roughly 100 W m^{-2}. This diurnal oscillation is a direct result of solar heating of the ice. At first the solar heating of the ice is less than the sensible heat flux, but as the ice grows thicker, the peak values of the solar heating become roughly comparable to the sensible flux. We see that peak values of the solar energy absorbed in the ice are lower than the sensible heat flux. The solar heating is comparable to the average net longwave radiation flux and greater than the latent heat flux.

Figure 4 summarizes the heat fluxes integrated over the 2.5-day observation period. During this period the theoretical simulations indicate that 30% (11 MJ m^{-2}) of the incident solar irradiance (38 MJ m^{-2}) was absorbed in the ice. Combined the solar heating in ice and water is roughly comparable in magnitude to the net longwave and is approximately two thirds of the turbulent fluxes. Our estimate of the total net heat for the lead ice was -47 MJ m^{-2}. This implies that solar heating of the ice reduced the net heat loss from the lead ice from -58 to -47 MJ m^{-2}, in effect reducing the ice growth by ~20%.

We can use the same radiative transfer model to examine the absorption of solar radiation in the ocean under the lead. Since the water was very clear, we assumed that scattering was negligible and that at any given wavelength the solar energy absorbed decreased exponentially with depth. Extinction coefficients for very clear water were used in the calculations [*Tyler and Smith*, 1970; *Grenfell*, 1979; *Smith and Baker*, 1981]. During the lead 3 observations, ~30% of the incident solar energy (11 MJ m^{-2}) was deposited in the ocean mixed layer and a few

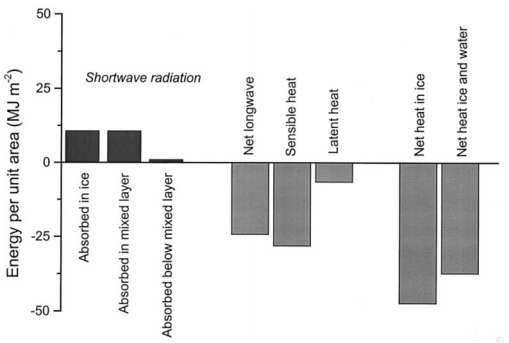

Figure 4. Summary of energy balance for lead 3. Values are integrated from 0900 UT on April 6 to 2400 UT on April 8.

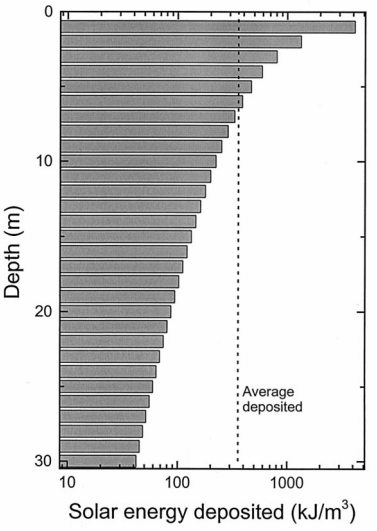

Figure 5. Solar energy deposited in the upper ocean under the young ice at lead 3. Values are integrated from 0900 UT on April 6 to 2400 UT on April 8.

percent (1 MJ m^{-2}) were absorbed below the mixed layer. Figure 5 shows the cumulative solar energy absorbed in 1-m-thick layers in the upper ocean under the lead as a function of depth. The energy absorbed deviates somewhat from an exponential decay since it is integrated over wavelength and the extinction coefficient is spectrally dependent. The solar energy deposited in the upper ocean decreased by orders of magnitude, from more than 1 MJ m^{-3} near the surface, to 0.1 MJ m^{-3} at a depth of 20 m, and to 0.01 MJ m^{-3} at a depth of 50 m.

While the solar heat was deposited nearly exponentially with depth, there was considerable vertical mixing [*McPhee and Stanton*, 1996; *Morison and McPhee*, 1998]. Because of the brine rejection from the freezing lead ice, vertical velocities were as high as 2.5 cm s^{-1}. There was also horizontal mixing and relative motion between the ice and ocean. The amount of solar radiation transmitted through the snow-covered multiyear ice is negligible ($\sim 10^{-5} F_r$) compared to that transmitted through lead ice ($> 10^{-1} F_r$). In a sense we can think of the lead ice as a window moving across the ocean. Since lead 3 was ~1 km wide and the relative ice-ocean velocity was 11 cm s^{-1} [*McPhee and Stanton*, 1996], a parcel of water would be exposed for ~9000 s (2.5 hours). Depending on the time of day, the amount of heating of the mixed layer during the 2.5-hour transit of the lead would range from a minimum of 0°C (at night) to a maximum of 0.007°C at solar noon. This maximum noontime solar heating is consistent with the range of ocean temperatures measured using masts [*McPhee and Stanton*, 1996] and from an autonomous underwater vehicle (AUV) [*Morison and McPhee*, 1998]. The radiative transfer-based estimate of the solar heat flux into the mixed layer at solar noon is 100 W m^{-2}, somewhat larger than the value of 70 W m^{-2} computed directly from ocean temperatures and vertical velocities [*McPhee and Stanton*, 1996]. The fact that the radiative transfer estimate is larger implies that there was horizontal spreading of the solar heat, which is consistent with the AUV measurements of *Morison and McPhee* [1998].

4. Conclusions

In springtime leads, relatively warm water is exposed to the cold atmosphere, resulting in large heat flux from the ocean to

the atmosphere and rapid ice growth in the lead. Ice thickness typically increased quickly, with 15–20 cm of growth in the first few days. We observed four modes of ice production in the leads: congelation growth, deformation, snow-ice formation, and frazil production. Congelation growth was dominant, though rafting was common and there was considerable snow-ice formation near the upwind lead edge. Large amounts of frazil ice were only found in wide leads under windy conditions.

This rapid ice growth was tempered by solar radiation. During spring, skies are often clear, and the incident solar irradiance is large. A strong diurnal solar signal was evident in the ice temperature observations and in the calculated estimates of the net heat flux. Theoretical calculations indicated that during the first few days of growth, 30% of incident solar irradiance was absorbed in the ice and 25% was absorbed in the upper ocean. Solar heating in the lead and ocean was roughly comparable to the net longwave flux over the lead ice and was about two thirds of the turbulent fluxes. This distribution of energy resulted in a 25% reduction in ice growth.

As evidenced in this study, solar radiation significantly affects ice production in springtime leads. There are still questions extant regarding the effect of solar radiation on ice production in springtime leads: in particular, regarding the influence of frost flowers. Frost flowers increase the albedo, tempering the impact of solar heating. In contrast, they also tend to insulate the ice, reducing growth [*Martin et al*., 1995, 1996]. Since opportunities for field studies of springtime leads are scarce, laboratory and modeling investigations provide feasible alternatives. For example, a one-dimensional thermodynamic model of young ice including a frost flower layer and a solar radiation source term could be used to investigate the competing effects of frost flowers on ice growth.

Acknowledgments. We thank N. Mulherin for his assistance in the field program, N. Perron for her efforts in the physical characterization of the ice samples, E. Andreas for helpful explanations of the turbulent fluxes, and C. Fairall for graciously providing the meteorological data for lead 3. This paper benefited greatly from the contributions of associate editor Humfrey Melling and three anonymous reviewers. This work was funded by the Office of Naval Research under the Arctic Leads Initiative and by the Department of Army Project on the optical properties of snow and ice.

References

Andreas, E. L., and B. A. Cash, Convective heat transfer over wintertime leads and polynas, *J. Geophys. Res*., *104*, 25,721–25,734, 1999.

Andreas, E. L., and B. Murphy, Bulk transfer coefficients for heat and momentum over leads and polynas, *J. Phys. Oceanogr*., *16*, 1875–1883, 1986.

Badgley, F. J., Heat budget at the surface of the Arctic Ocean, in *Proceedings of the Symposium on the Arctic Heat Budget and Atmospheric Circulation*, edited by J. O. Fletcher, pp. 267–277, Rand, Santa Monica, Calif., 1966.

Bauer, J., and S. Martin, A model of grease ice growth in small leads, *J. Geophys. Res*., *88*, 2917–2925, 1983.

Dunkle, R. V., and J. T. Bevans, An approximate analysis of the solar reflectance and transmittance of a snow cover, *J. Meteorol*., *13*, 212–216, 1957.

Gow, A. J., D. A. Meese, D. K. Perovich, and W. B. Tucker III, The anatomy of a freezing lead, *J. Geophys. Res*., *95*, 18,221–18,232, 1990.

Grenfell, T. C., The effects of ice thickness on the exchange of solar radiation over the polar oceans, *J. Glaciol*., *22*, 305–320, 1979.

Grenfell, T. C., and G. A. Maykut, The optical properties of ice and snow in the Arctic Basin, *J. Glaciol*., *18*, 445–463, 1977.

Grenfell, T. C., et al., Evolution of Electromagnetic-Signatures of Sea Ice From Initial Formation Through the Establishment of Thick First-Year Ice, *IEEE Trans. Geosci. Remote Sens*., *36*, 1642–1654, 1998.

Martin, S., and P. Kauffman, A field and laboratory study of wave damping by grease ice, *J. Glaciol*., *27*, 283–313, 1981.

Martin, S., R. Drucker, and M. Fort, A laboratory study of frost flower growth on the surface of young sea ice, *J. Geophys. Res*., *100*, 7027–7036, 1995.

Martin, S., Y. Yu, and R. Drucker, The temperature dependence of frost flower growth on laboratory sea ice and the effect of the flowers on infrared observations of the surface, *J. Geophys. Res*., *101*, 12,111–12,125, 1996.

Maykut, G. A., Energy exchange over young sea ice in the central Arctic, *J. Geophys. Res*., *83*, 3646–3658, 1978.

Maykut, G. A., Large-scale heat exchange and ice production in the central Arctic, *J. Geophys. Res*., *87*, 7971–7985, 1982.

McPhee, M. G., and T. P. Stanton, Turbulence in the statically unstable oceanic boundary layer under Arctic leads, *J. Geophys. Res*., *101*, 6409–6428, 1996.

Morison, J. H., and M. G. McPhee, Lead convection measured with an autonomous underwater vehicle, *J. Geophys. Res*., *103*, 3257–3282, 1998.

Morison, J. H., M. G. McPhee, T. Curtin, and C. A. Paulson, The oceanography of winter leads, *J. Geophys. Res*., *97*, 11,199–11,218, 1992.

Nakawo, M., and N. K. Sinha, Growth rate and salinity profile of first-year sea ice in the high Arctic, *J. Glaciol*., *27*, 315–330, 1981.

Perovich, D. K., Theoretical estimates of light reflection and transmission by spatially complex and temporally varying sea ice covers, *J. Geophys. Res*., *95*, 9557–9567, 1990.

Perovich, D. K., and T. C. Grenfell, Laboratory studies of the optical properties of young sea ice, *J. Glaciol*., *27*, 331–346, 1981.

Perovich, D. K., and J. A. Richter-Menge, Surface characteristics of lead ice, *J. Geophys. Res*., *99*, 16,341–16,350, 1994.

Pinto, J. O., and J. A. Curry, Atmospheric convection plumes emanating from leads, 2, Microphysical and radiative processes, *J. Geophys. Res*., *100*, 4633–4642, 1995.

Pinto, J. O., J. A. Curry, and K. L. McInnes, Atmospheric convection plumes emanating from leads, 1, Thermodynamic structure, *J. Geophys. Res*., *100*, 4621–4632, 1995.

Ruffieux, D., P. O. G. Perrson, C. W. Fairall, and D. E. Wolfe, Ice pack and lead surface energy budgets during LEADEX 1992, *J. Geophys. Res*., *100*, 4593–4612, 1995.

Schnell, R. C., R. G. Barry, M. W. Miles, E. L. Andreas, L. F. Radke, C. A. Brock, M. P. McCormick, and J. L. Moore, Lidar detection of leads in Arctic sea ice, *Nature*, *339*, 530–532, 1989.

Schwerdtfeger, P., The thermal properties of sea ice, *J. Glaciol*., *4*, 789–807, 1963.

Smith, R. C., Optical properties of the Arctic upper water, *Arctic*, *26*, 303–313, 1973.

Smith, R. C., and K. S. Baker, Optical properties of the clearest natural waters (200–800 nm), *Appl. Opt*., *20*, 177–184, 1981.

Smith, S. D., R. D. Muench, and C. H. Pease, Polynyas and leads: An overview of physical processes and environment, *J. Geophys. Res*., *95*, 9461–9479, 1990.

The LeadEx Group, The LeadEx Experiment, *Eos Trans. AGU*, *74*, 393–397, 1993.

Tucker, W. B., III, A. J. Gow, and W. F. Weeks, Physical properties of summer sea ice in the Fram Strait, *J. Geophys. Res*., *92*, 6787–6803, 1987.

Tyler, J. E., and R. C. Smith, *Measurements of Spectral Radiance Underwater*, Gordon and Breach, Newark, N. J., 1970.

Untersteiner, N., On the mass and heat budget of Arctic sea ice, *Arch. Meteorol. Geophys. Bioklim*., *Ser. A, 12*, 151–182, 1961.

Weeks, W. F., and S. F. Ackley, The growth, structure, and properties of sea ice, in *The Geophysics of Sea Ice*, edited by N. Untersteiner, pp. 1–164, Plenum, New York, 1986.

D. K. Perovich and J. A. Richter-Menge, U.S. Army Cold Regions Research and Engineering Laboratory, Hanover, NH 03755-1290. (perovich@crrel.usace.army.mil)

(Received July 1, 1998; revised November 9, 1999; accepted December 3, 1999.)